EXPERIMENTS ON A SLENDER BODY OF REVOLUTION MOVING NEAR A WALL

by

Richard Francis Elliott
May 23, 1969

EXPERIMENTS ON A SLENDER BODY OF REVOLUTION MOVING NEAR A WALL

by

RICHARD FRANCIS ELLIOTT
ENSIGN, UNITED STATES NAVY
B.S. UNITED STATES NAVAL ACADEMY
(1968)

Submitted in Partial Fulfillment of the
Requirements for the Degree of
Master of Science in Naval Architecture
and Marine Engineering
at the
MASSACHUSETTS INSTITUTE OF TECHNOLOGY
May, 1969

Signature of Author: _____
Department of Naval Architecture and Marine Engineering, May 23, 1969

Certified by: _____
Thesis Supervisor

Accepted by: _____
Chairman, Departmental Committee on Graduate Students

EXPERIMENTS ON A SLENDER BODY OF REVOLUTION MOVING NEAR A WALL

by

RICHARD FRANCIS ELLIOTT

Submitted to the Department of Naval Architecture and Marine Engineering on May 23, 1969, in partial fulfillment of the requirements for the Master of Science degree in Naval Architecture and Marine Engineering.

ABSTRACT

Experiments were conducted on body of revolution immersed in a fluid and moving parallel to the wall in order to determine the force and moment on the body due to the presence of the wall. Data is compared with the results of previous theoretical work, which were solved for the body in question. An evaluation is made of both the test values and those derived from the theory. Recommendations for the future study in this and related fields is also included.

Thesis Supervisor: John Nicholas Newman,
Associate Professor of Naval Architecture

TABLE OF CONTENTS

LIST OF FIGURES

LIST OF TABLES

note: Table XVIII - omitted

I. INTRODUCTION

It has been said that a scientist seeks knowledge purley for knowledge's sake. He spends his life trying to determine the laws of nature that govern the world about him, often penetrating deep into the unknown and never quite sure of the happenings that will transpire. The engineer, on the other hand, is interested in applying the knowledge already acquired to the physical everyday world. He is interested in understanding phenomena only to the extent that it aids him in mastering his environment. It is evident that these two professions must exist and work hand in hand if man is to continue to advance.

As the scientist extends man's knowledge, the engineer becomes more able to predict how mechanical systems will perform. Naval architecture is almost as old as man himself, but only recently has true theory entered upon the scene. The field that was once considered an art and later governed by strictly empirical laws is now entering the realm of true science. The areas in which theory can be applied are increasing rapidly.

One such problem that may be tackled in this nature

is the force that acts on the body when it moves through a fluid close to the wall. This has always been a problem to mariners when moving in shallow waters and narrow channels or when coming along side a wall or pier, but with the advent of the second generation or maneuvering deep submergence vehicles it has taken on a new inportance. Because they operate in close proximity to the bottom and are limited in power, a comprehension of the forces involved and an ability to predict them becomes critical.

The problem that is encountered may be simply explained as a venturi effect. The reduction of flow area between the body and the wall causes an acceleration of the fluid and, from Bernoulli's principle, results in a pressure decrease on the wall side of the body. This differential in pressure gives rise to a net "suction" force toward the wall. In addition were this force to act through a point other than the center of gravity of the body, a moment would also be produced.

The theoretical problem is greatly simplified if the body selected for study is a body of revolution. The modern submarine is, for the most part, a true body of this form. For purposes of analysis, the under water hull form of a ship may many times be considered as the lower half of such a body.

This paper is a report on an experimental investiga-

tion into the force and moment on a body of revolution moving parallel and close to a wall. The results of these experiments are given in Section III and are compared with present theory in Section IV.

There have been many papers published that consider the potential flow generated by a particular class of bodies of revolution, the spheroid. While the material does not apply strictly to the problem at hand, it was an essential tool for generating the theory which was investigated for this report.

Lagally [1] developed a method by which the force and moment acting on a body in a steady, inviscid potential flow could be determined. This theory was generalized by Cummins [2] for a time-varying potential flow. Landweber and Macagno [3] considered the case of an elongated body.

An earlier work dealing with the present problem was published by Eisenberg [4] in 1950. Assuming that the velocity potential generated by the body-wall system could be replaced by that due to the spheroid plus a potential due to an image spheroid, both in an infinite fluid, he calculated the pressure distribution on the object in question. It is an easy task to integrate this pressure distribution over the body and thus determine the force and moment. Although experimental evi-

dence supported this development, the presence of an induced velocity on one body due to the other, and visa versa, was never taken into account. Thus, Eisenberg's theory may be considered to more closely approximate the real problem when the spheroid is at a distance from the wall, where the induced velocities are negligible.

Although the latest work in the field is by James [5], it was not circulated prior to this writing. Therefore, an earlier report by Newman [6], theoretical in nature, is the one considered by this report for investigation. Newman attempted to predict the force and moment on any body of revolution (within the limits of certain assumptions) moving parallel to and in close proximity of a plane wall. The development used in this theory is outlined below.

In order that the problem may lend itself to an analytical approach it is necessary to idealize the actual situation. The fluid must be considered inviscid, incompressible and of infinite expance except at the wall. This is required so that potential theory may be used and frictional forces neglected. The problem is simplified if slender body theory is used. Thus the body must be slender and, as mentioned above, in close proximity to the wall.

As shown in fig. 1, the body is considered to be situated in a Cartesian coordinate system at $(0,0,z_o)$

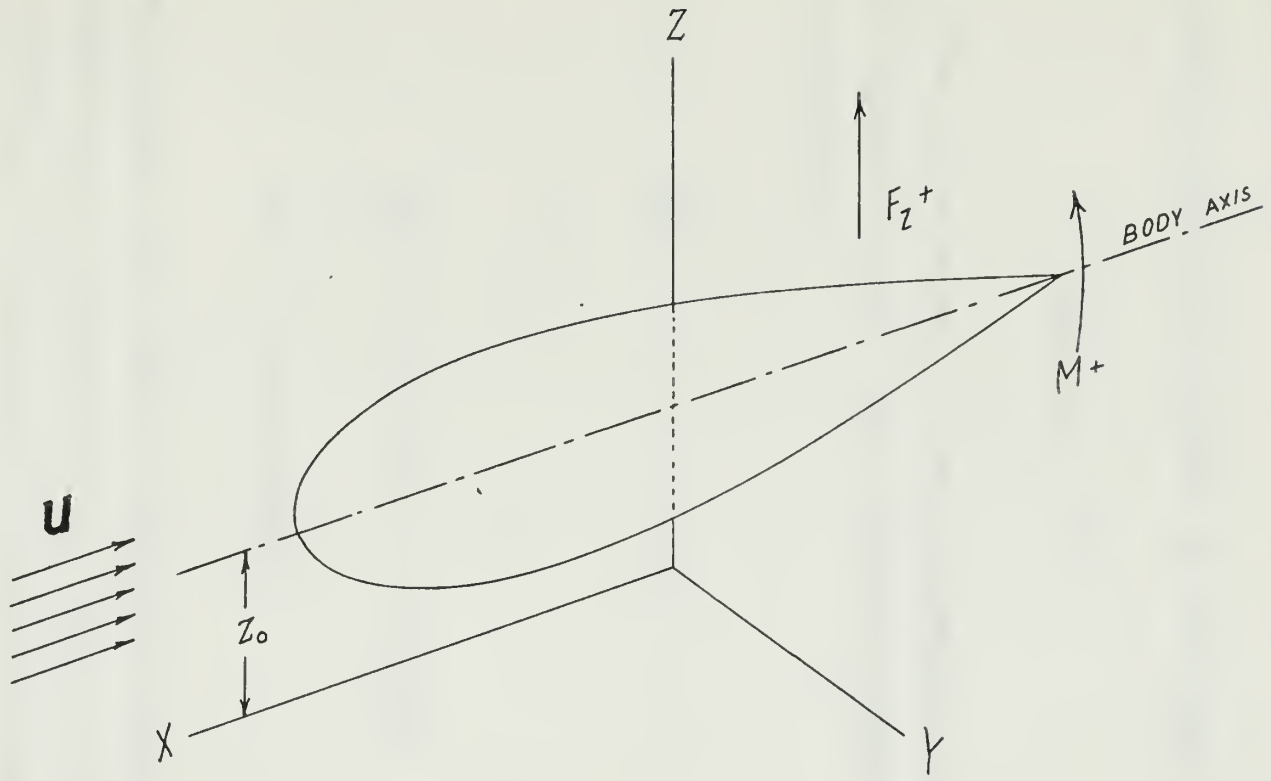

Fig. 1 Coordinate System

with the fluid flowing past with a free stream velocity $-U\vec{i}$. It is required that the radius of revolution, $r_o(x)$, be a smooth continuous function of x, and go to zero at the nose and tail.

Defining the velocity field by the vector

$$V = \nabla\phi(x,y,z) - U\vec{i} \quad , \qquad [1]$$

where ϕ is the potential of the perturbation flow and U the free stream velocity, the following boundary conditions must be satisfied:

$$\frac{\partial\phi}{\partial z} = 0 \quad \text{at} \quad z = 0$$

$$\nabla^2\phi = 0$$

$$\frac{\partial\phi}{\partial\bar{n}} = U \cos(\bar{n},x) = - U\, r_o'(x)$$

$$\nabla\phi = 0 \quad \text{at infinity}$$

From slender body theory, the local potential close to the body may be considered as the sum of a two dimensional potential in the cross flow plane plus some function of x.

$$\phi(x,y,z) \cong \phi_{2D}(y,z;x) + f(x) \qquad [2]$$

The two dimensional potential may be found as

$$\phi_{2D}(y,z;x) = -\frac{1}{4\pi} US'(x) \log \left\{ \left[y^2 + (z - a)^2 \right] \left[y^2 + (z + a)^2 \right] \right\} \qquad [3]$$

where

$$a(x) = \left[z_o^2 - r_o(x)^2 \right]^{\frac{1}{2}}$$

The three dimensional potential associated with this is

$$\phi(x,y,z) = \frac{1}{4\pi} U \int_{-\frac{L}{2}}^{\frac{L}{2}} S'(\xi) \left\{ \left[(x - \xi)^2 + y^2 + (z - a)^2 \right]^{-\frac{1}{2}} + \left[(x - \xi)^2 + y^2 + (z + a)^2 \right]^{-\frac{1}{2}} \right\} d\xi \qquad [4]$$

Lagally's theorem may be employed to determine the vertical force and moment acting on the body, or

$$F_z = \frac{1}{4\pi} \rho U^2 \int_{-\frac{L}{2}}^{\frac{L}{2}} S'(x) \left\{ \frac{\partial}{\partial z} \int_{-\frac{L}{2}}^{\frac{L}{2}} S'(\xi) \left[(x - \xi)^2 + (z + a)^2 \right]^{-\frac{1}{2}} d\xi \right\} dx \Bigg|_{z = a(x)} \qquad [5]$$

and

$$M_y = \frac{1}{4\pi} \rho U^2 \int_{-\frac{L}{2}}^{\frac{L}{2}} S'(x) \left\{ \frac{\partial}{\partial z} \int_{-\frac{L}{2}}^{\frac{L}{2}} S'(\xi) \left[(x - \xi)^2 + (z + a)^2 \right]^{-\frac{1}{2}} d\xi \right\} x dx \Bigg|_{z = a(x)} \qquad [6]$$

Evaluating the problem from slender body theory and

replacing S'(x) by

$$2\pi r_o(x) r_o'(x)$$

the final results may be obtained as

$$F_z = -\pi\rho U^2 \int_{-\frac{L}{2}}^{\frac{L}{2}} \left[r_o(x) r_o'(x)\right]^2 \left\{ z_o^2 - \left[r_o(x)\right]^2 \right\}^{-\frac{1}{2}} dx \qquad [7]$$

and

$$M_y = \pi\rho U^2 \int_{-\frac{L}{2}}^{\frac{L}{2}} \left[r_o(x) r_o'(x)\right]^2 \left\{ z_o^2 - \left[r_o(x)\right]^2 \right\}^{-\frac{1}{2}} x\,dx \qquad [8]$$

Equations [5] , [6] , [7] and [8] will be evaluated for the shape tested for this report and compared with experimental results in Section IV.

II. EQUIPMENT DESIGN AND TEST PROCEDURE

As was mentioned earlier, the theory used to predict the force and moment on a body moving near a wall required an idealized situation. While this could never be achieved in a real environment, every effort within the scope of this work was taken to insure that the test situation would conform as close as possible to the theoretical problem. The equipment used and the procedure followed are outlined below.

All experiments which are reported in this paper were conducted in the M.I.T. propeller tunnel. This was a closed loop system in which the body was held stationary and the water forced to flow. Circulation was achieved with the aid of an impeller located down stream of the 20 in. by 20 in. test section. Parallel, uniform flow was approximated by insertion of a honeycomb lattice and three screens upstream of the test section. Although the only method available for calculating water speed was the measurement of the impeller RPM, later calibration showed this procedure to be fairly accurate at speeds over 10 ft./sec. Therefore, only the data obtained from experiments in flows greater than this speed are reported.

The device available to measure the force and moment on the body was a newly constructed dynamometer, a schematic diagram of which is shown in fig. 2. This apparatus consisted of five Lebow load cells arranged to read drag at two locations, force perpendicular to the wall, lateral force and moment about the axis perpendicular to the wall. For the purpose of this report, only the two drag forces and the attraction toward the wall were considered. These will henceforth be referred to as inner drag, outer drag, and lift. The two drag cells measured the total drag and determined the pitching moment.

It became obvious as the experiments progressed that the dynamometer system was not ideally suited for measurement of the forces to be encountered in this situation. The apparatus was designed to record forces of a much larger magnitude. For example, the lift load cell was rated at 100 lbs. maximum capacity, while the inner and outer drag cells were designed for 500 lbs. and 200 lbs. full load, respectively. Naturally, the supporting structure was also designed with large loading in mind. The outputs from various cells were fed into Lebow model 66 transducers with digital outputs of 1,000 counts. Although insertion of 0.05 mv./v. span boards in the transducers resulted in a resolution of $\pm$ 0.025 lbs., $\pm$ 0.125 lbs., and $\pm$ 0.050 lbs., respectively, the induced cross forces and cross torques among the cells plus an inherent

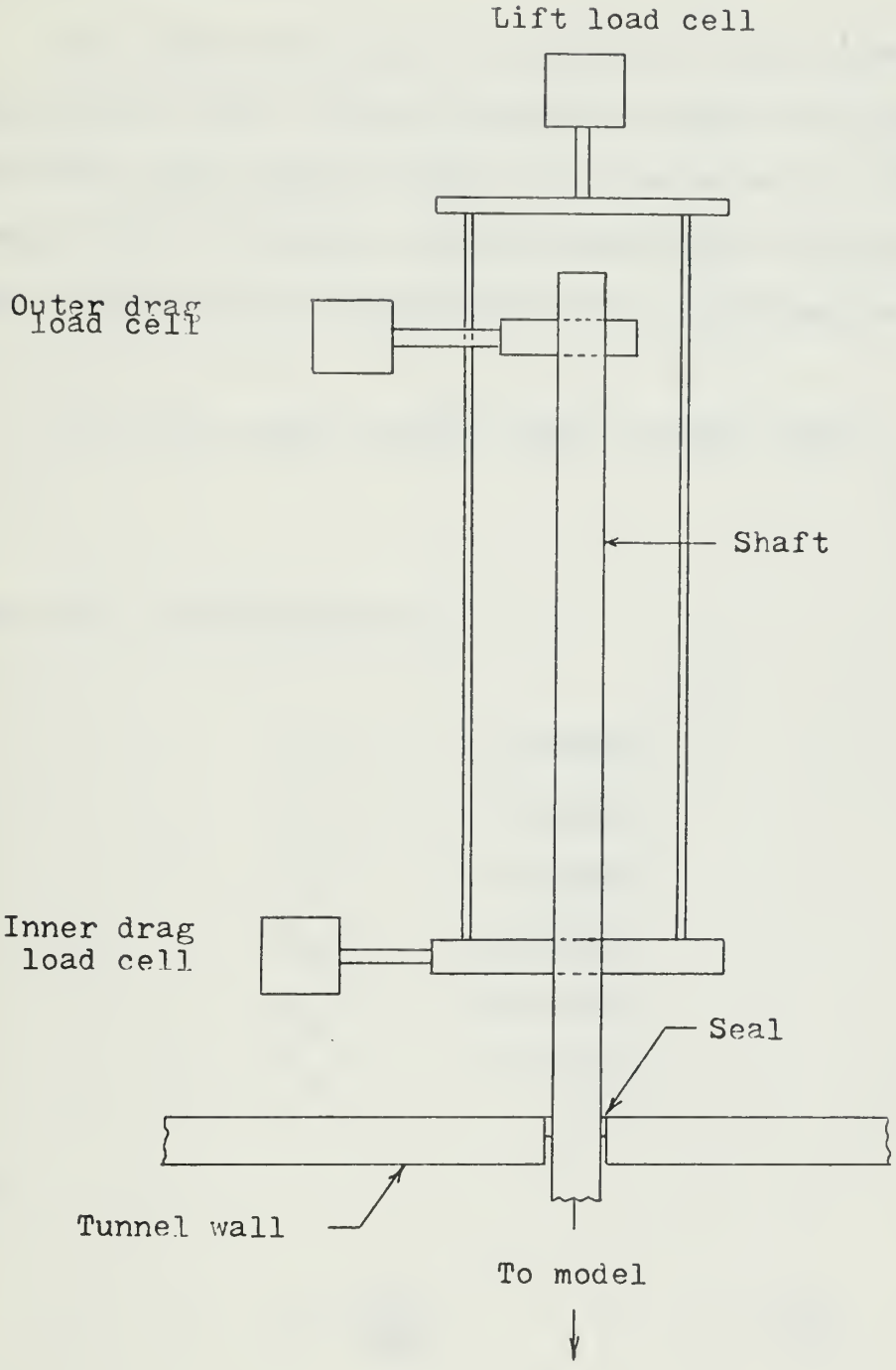

Fig. 2 Dynamometer Schematic

hysteresis of the total physical system induced errors in the measurements.

The body form chosen to evaluate in the experiments was derived from a shape previously tested for drag by the David Taylor Model Basin and reported on in DTMB report C-297 of April, 1950 (unclassified). The streamwise profile may be described by the following euqation:

$$Y^2 = a_1X + a_2X^2 + a_3X^3 + a_4X^4 + a_5X^5 + a_6X^6 \qquad [9]$$

where the coefficients are

$$a_1 = + 1.000000$$
$$a_2 = + 0.837153$$
$$a_3 = - 8.585996$$
$$a_4 = +14.075954$$
$$a_5 = -10.542535$$
$$a_6 = + 3.215422$$

and

$$Y = \frac{r(x)}{D_{max}} \quad , \quad X = \frac{x}{L}$$

The term r(x) is the local radius of revolution, x is the

distance from the nose, D_{max} the maximum diameter, and L the overall length.

The model itself was constructed of lucite, designed at an L of 24.5 in. and a D_{max} of 3.5 in. occurring at an x of 9.80 in. Thus, it possessed an L/D of 7.0. It was hoped that the slenderness and a fine stern would prevent most vortex shedding plus enhance the applicability of slender body theory. Observation of the model in test situations demonstrated that very few vorticies were generated.

The most difficult design problen encountered was the method of supporting the body. Naturally the most ideal situation possible would be to place no obstruction between the wall and the model. This was unobtainable from a strength consideration, however. It was therefore necessary to place a 3/4 in. diameter support shaft between the body and the wall and consider the wall containing the dynamometer as the infinite wall of the theory. The error that was produced in the data, even though a fairing was placed aroung the shaft to reduce the effect of the obstruction, is discussed in Section IV.

Dead weight calibration was considered to be the most reliable method and was applied for the analysis of the dynamometer system. A series of weights were hung

vertically to apply both a lift force and pitching moments. Weights hung over a pulley produce a drag and a second moment. It was hoped that the true effect of the forces and moments could be determined so that the cross forces and cross torques might be eliminated from the final data. Because the system was new and this procedure of calibration never attempted before, the accuracy of this method was not entirely predictable.

The execution of the experiments adhered to a precise format. After installation of the model in the test section, all recording instruments were zeroed and the pressure in the tunnel was recorded. The flow was then initiated and its speed slowly increased to a predetermined value. At such time as the flow was considered steady, all force readings were recorded, as was the pressure. (Knowledge of the change in total pressure was essential. Because the forces involved were small, any reduction in pressure would cause a relatively large force away from the wall.) The velocity was increased again and the procedure repeated. Eight incramental values of flow speed between 10 ft./sec. and 19 ft./sec. were selected for investigation; these velocities were also duplicated and readings taken as the flow was decreased.

After the impeller was shut down and all the data

recorded, the tunnel was drained and the model removed. It was then necessary to reduce the span of the fairing. The body was replaced in the test section, closer to the wall, and the entire format repeated. Values of z_o/r_o max. were decreased from a maximum of 2.43 to a minimum of 1.02. For values of 1.18 and 1.02 it was necessary to remove the fairing entirely.

The results of these experiments are recorded in Section III.

III. RESULTS

As was mentioned earlier, the dynamometer was plagued with cross force and cross torque errors plus a hysteresis of the entire system. Had the force measurement system been designed to read to a much smaller maximum capacity, the resolution would have been far superior and the inaccuracies more readily calculable. With the available system, however, a procedure was followed that would eliminate, it was hoped, the major effect of these inherent errors. This format is outlined in detail in Appendix 1.

Because the force and moment on a body moving parallel to a wall vary with both the water speed and water density, it is much easier to work with coefficients of force and moment. We will define these coefficients as follows:

$$C_f = - \frac{F_z}{\frac{1}{2}\rho U^2 L^2} \qquad \text{and} \qquad C_m = \frac{M_y}{\frac{1}{2}\rho U^2 L^3}$$

The computed values of C_f for all of the test model may be found in Tables I through XII at the end of this section. It should be noticed that a sign of C_f has

been reversed from that of F_z. Thus a positive coefficient indicates an attraction toward the wall. The actual values of lift, which are not essential for analysis here, are tabulated in Appendix 2.

It is obvious that the lift force did not maintain a constant direction throughout the experiments, as the theory predicts. The reasons for this discrepency are considered in Section IV. Also to be found in the next section is an explanation of how the lift error complicates the solution for the moments to such an extent that they are completely meaningless. For this reason, values of C_m are omitted from this section. The recorded values of the moments, however, are included in Appendix 2.

In order to compare the actual data with the aforementioned theory, equations [5], [6], [7], and [8] were solved using approximation methods. Values of C_f and C_m in the first two equations were found by means of the trapazoidal rule. The last two were integrated with Simpson's Rule. The values thus derived are contained in Tables XIII through XVI.

Reference to the tables of experimental C_f shows that a constant value of the coefficient was not maintained for each value of z_o/r_o max., as should be the case. The most logical way to analyze this data, there-

fore, would be to average the results at each distance from the wall. To make the effects of hysteresis and zero shifting more evident, it was decided to average the values recorded as the flow speed was increased separately from those taken during the velocity reduction. Thus, the repeatability of data will be more or less exposed. These averaged values are listed in Table XVII.

So that a ready comparison of the experimental results and the theory can be made, all final values of C_f are plotted in graph form in fig. 3. This also provides an opportunity to observe discrepencies between the theoretical values. For this reason, the analytical values of C_m are plotted in fig. 4.

The following section contains an analysis of all the data presented here for report.

Fig. 3. TEST AND THEORETICAL DATA

C_F VS z_o/r_o max.

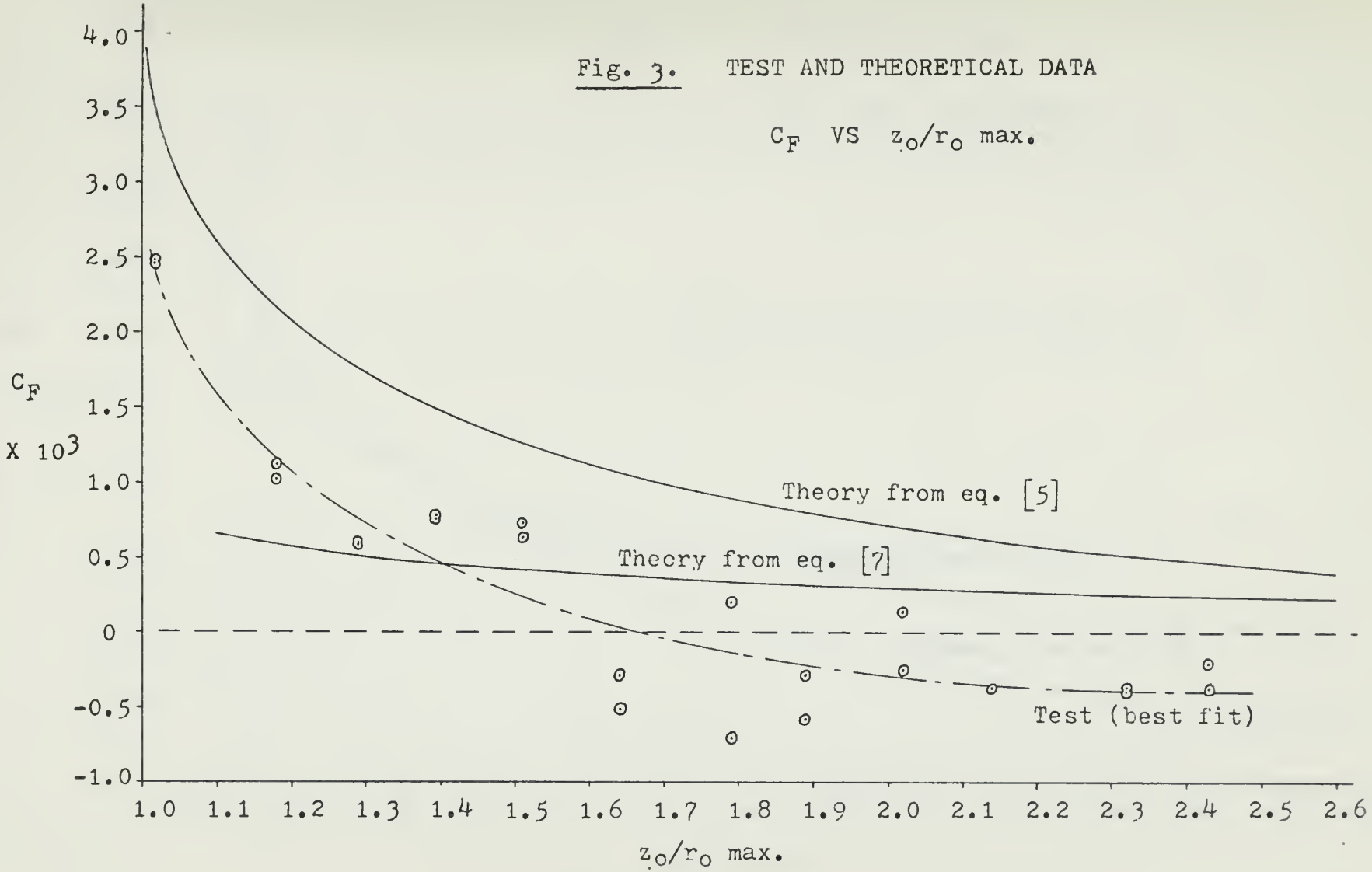

Fig. 4 THEORETICAL DATA

C_m vs z_o/r_o max.

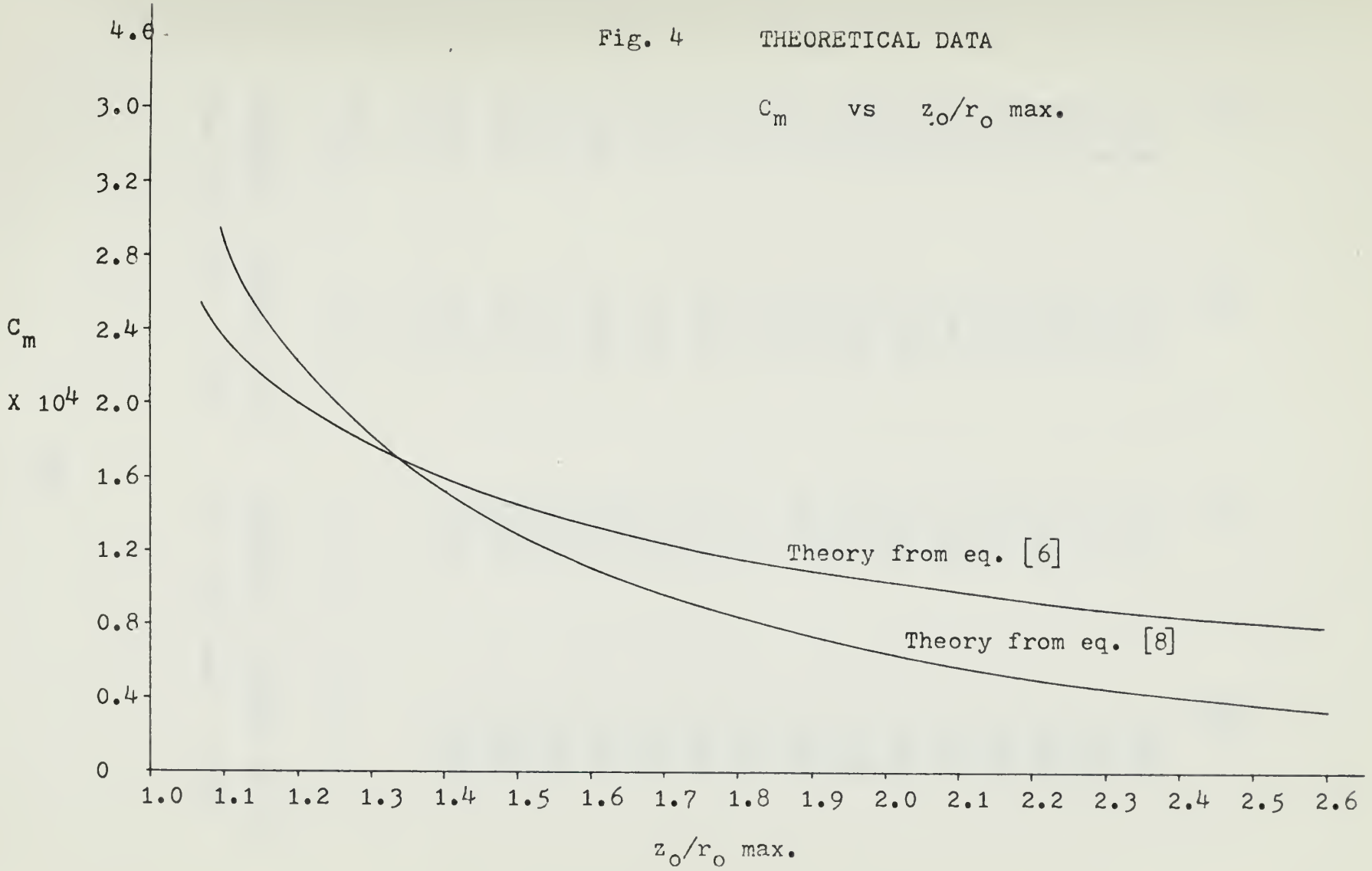

$\frac{U}{-}$	$\frac{C_f}{}$	$\frac{U}{-}$	$\frac{C_f}{}$
11.4	-.343	10.7	-.284
12.3	-.356	11.9	-.252
12.9	-.254	13.3	-.268
13.9	-.280	14.5	-.405
14.9	-.424	15.8	-.495
15.8	-.308	17.0	-.505
16.9	-.298	18.1	-.472
17.4	-.324	18.6	-.480
18.5	-.331	17.9	-.505
17.7	-.295	17.1	-.504
16.9	-.220	15.6	-.387
15.6	-.170	14.6	-.344
14.8	-.186	13.3	-.210
13.3	-.123	12.0	-.282
12.4	-.054	10.9	-.200
11.5	-.157		
10.5	-.180		

TABLE I. Values of C_f for z_o/r_o max. = 2.43

TABLE II. Values of C_f for z_o/r_o max. = 2.32

$\frac{U}{-}$	$\frac{C_f}{}$
10.7	-.413
12.2	-.481
13.4	-.477
14.4	-.461
15.4	-.425
16.9	-.396
18.0	-.189
18.6	-.008

TABLE III. Values of C_f for z_o/r_o max. = 2.14

$\frac{U}{-}$	$\frac{C_f}{}$
10.7	-.301
12.0	-.355
13.1	-.394
14.4	-.364
15.9	-.454
16.9	-.158
18.0	-.061
18.6	+.024
17.9	+.033
16.9	+.004
15.8	+.125
14.4	+.244
13.0	+.174
12.0	+.215
10.7	+.313

TABLE IV. Values of C_f for z_o/r_o max. = 2.02

$\frac{U}{-}$	$\frac{C_f}{-}$	$\frac{U}{-}$	$\frac{C_f}{-}$
10.7	- .111	10.5	+.125
12.1	- .197	11.8	+.190
13.1	- .199	13.0	+.228
14.6	- .240	14.3	+.065
15.6	- .280	15.5	-.006
16.7	- .485	16.7	-.106
18.0	- .280	18.0	-.164
18.6	- .487	18.6	-.174
18.0	- .322	18.0	-.136
16.7	- .389	16.7	-.129
15.4	- .495	15.5	-.081
14.6	- .636	14.3	-.002
13.1	- .434	13.0	-.010
12.1	-1.021	11.8	-.005
10.7	- .482	10.5	-.026

TABLE V. Values of C_f for z_o/r_o max. = 1.89

TABLE VI. Values of C_f for z_o/r_o max. = 1.79

U	C_f	U	C_f
10.5	-.011	10.5	+.784
11.8	+.081	11.8	.675
13.0	+.075	13.0	.660
14.3	-.042	14.3	.643
15.5	-.134	15.5	.576
16.7	-.071	16.7	.570
18.0	-.081	18.0	.591
18.6	-.053	18.6	.601
18.0	-.033	18.0	.633
16.7	-.049	16.7	.609
15.5	-.043	15.5	.670
14.3	-.033	14.3	.720
13.0	-.019	13.0	.751
11.8	-.164	11.8	.866
10.5	-.015	10.5	.945

TABLE VII. Values of C_f for z_o/r_o max. = 1.64

TABLE VIII. Values of C_f for z_o/r_o max. = 1.51

$\frac{U}{-}$	$\frac{C_f}{—}$	$\frac{U}{-}$	$\frac{C_f}{—}$
10.5	+.881	10.5	+.306
11.8	.800	11.8	.466
13.0	.828	13.0	.635
14.3	.825	14.3	.859
15.5	.787	15.5	.723
16.7	.668	16.7	.615
18.0	.623	18.0	.659
18.6	.617	18.6	.607
18.0	.609	18.0	.584
16.7	.685	16.7	.520
15.5	.685	15.5	.548
14.3	.649	14.3	.595
13.0	.840	13.0	.541
11.8	.960	11.8	.528
10.5	.960	10.5	.804

TABLE IX. Values of C_f for z_o/r_o max. = 1.39

TABLE X. Values of C_f for z_o/r_o max. = 1.29

$\frac{U}{-}$	$\frac{C_f}{--}$	$\frac{U}{-}$	$\frac{C_f}{--}$
10.5	+1.342	10.5	+2.458
11.8	1.080	11.8	2.359
13.0	1.040	13.0	2.375
14.3	1.068	14.3	2.495
15.5	1.120	15.5	2.442
16.7	1.100	16.7	2.500
18.0	1.090	18.0	2.505
18.6	1.088	18.6	2.555
18.6	1.126	18.6	2.470
18.0	1.068	18.0	2.521
16.7	1.118	16.7	2.438
15.5	1.120	15.5	2.467
14.3	1.031	14.3	2.426
13.0	.935	13.0	2.423
11.8	.930	11.8	2.556
10.5	.926	10.5	2.522

RABLE XI. Values of C_f for z_o/r_o max. = 1.18

TABLE XII. Values of C_f for z_o/r_o max. = 1.02

z_o/r_o max.	C_f
1.1	2.6009
1.2	2.0825
1.3	1.7349
1.4	1.4783
1.5	1.2788
1.6	1.1187
1.7	.9871
1.8	.8771
1.9	.7839
2.0	.7041
2.1	.6351
2.2	.5751
2.3	.5224
2.4	.4760
2.5	.4349
2.6	.3982
2.7	.3656

TABLE XIII. Values of C_f derived from eq. [5] X 10^3.

z_o/r_o max.	C_f
1.1	.6602
1.2	.4124
1.3	.3619
1.5	.4110
1.7	.3519
1.9	.3089
2.1	.2757
2.3	.2493
2.5	.2277
2.7	.2096
2.9	.1943

TABLE XIV. Vlaues of C_f derived from eq. [7] X 10^3.

z_o/r_o max.	C_m
1.1	2.8662
1.2	2.2404
1.3	1.8230
1.4	1.5186
1.5	1.2856
1.6	1.1017
1.7	.9532
1.8	.8312
1.9	.7297
2.0	.6442
2.1	.5717
2.2	.5095
2.3	.4559
2.4	.4094
2.5	.3689
2.6	.3333
2.7	.3021

TABLE XV. Values of C_m derived from eq. [6] X 10^4.

z_o/r_o max.	C_m
1.1	2.3580
1.2	2.0078
1.3	1.7705
1.5	1.4530
1.7	1.2416
1.9	1.0883
2.1	.9708
2.3	.8773
2.5	.8094
2.7	.7373
2.9	.6832

TABLE XVI. Values of C_m derived from eq. [8] X 10^4.

z_o/r_o max.	C_f	
2.43	-.377	-.214
2.32	-.395	-.364
2.14	-.365	
2.02	-.258	+.142
1,89	-.283	-.534
1.79	+.198	-.704
1.64	-.295	-.511
1.51	+.638	+.725
1.39	+.786	+.757
1.29	+.609	+.591
1.18	+1.118	+1.033
1.02	+2.467	+2.480

TABLE XVI. Values of C_f for values of z_o/r_o max.

IV. DISCUSSION OF RESULTS

Reference to fig. 3 shows that not only did the experimental values of C_f fall below those predicted by theory, but also they became negative in many cases, indicating a force away from the wall. This section will attempt to uncover the reasons why this is so. An explanation of the inability to calculate C_m will also be given. Finally, a discussion of the discrepency between values of C_f and of C_m as predicted by the two forms of the theory will be included in this section.

After the cross force and cross torque errors had been eliminated from the data, it was necessary to correct for any shift in the instrument zero during the test run. Assuming that this varied in some sort of constant manner, a linearly increasing or decreasing alteration was applied to the values of data. It is impossible to estimate exactly what transpired during testing, but this procedure should be considered the very best estimate.

Another error which became evident was that due to a pressure drop. From Bernoulli's equation an increase in velocity in the test section gives rise to this decrease. Were this differential to happen in a static

situation, the force exerted on the support shaft could be easily calculated. In the dynamic situation, however, it is impossible to measure the exact pressure at the exposed end of the shaft where the force is acting, because of the acceleration of the flow past the body. It was necessary, therefore, to assume that the pressure was the same everywhere and solve for the force with data taken at a pressure tap located at the mid-depth of the test section.

Any other sources of error present in the experiments are not readily discernable. However, reference to basic hydrodynamic theory might give an insight into the reasons why values do not conform to the theory prediction. Because the exact physical conditions are not known, it is impossible to calculate the actual magnitude of these errors.

Any slight angle of attack that the body might have had, due to either improper mounting or a non-uniform flow, would produce an error. A lift force of the same order of magnitude as the forces measured is obtainable with a fraction of a degree of angle of attack.[1] This is incalculable within the scope of this paper, but it could very well explain the negative lift.

A source of error could also be readily expected from the supporting shaft. During the experiments it

was noted that the flow was extremely turbulent around this device, even though a fairing had been added. It is evident that this would have an effect on the readings, but what type of effect is not apparant. Most likely the flow was decreased ahead of the strut and increased as it passed the strut. This would correspond to an increase in pressure ahead and a decrease at the strut. Such conditions would effect the lift of the system.

It is not attempted in this paper to calculate the effect of these errors on the data. The results fall below the theoretical curves in fig. 3, and it will suffice to say that the sources of error noted above, when coupled together, could easily produce the discrepency. It is unfortunate that all errors could not be eliminated and the theory more adequately evaluated.

Even so, it can be noted that a curve-fit through the data points would possess the same curve shape as the theoretical data derived from eq. [5] . If it is assumed that the errors are independent of the distance from the wall, a vertical shift of the data curve so that no value is negative shows a much better conformity to theory. This is shown in fig. 5. It is hypothesized that this curve more nearly represents the values of lift due to the wall effect.

As was mentioned in Section III, the moment data

Fig. 5 Test and Theoretical Data

C_f vs z_o/r_o max.

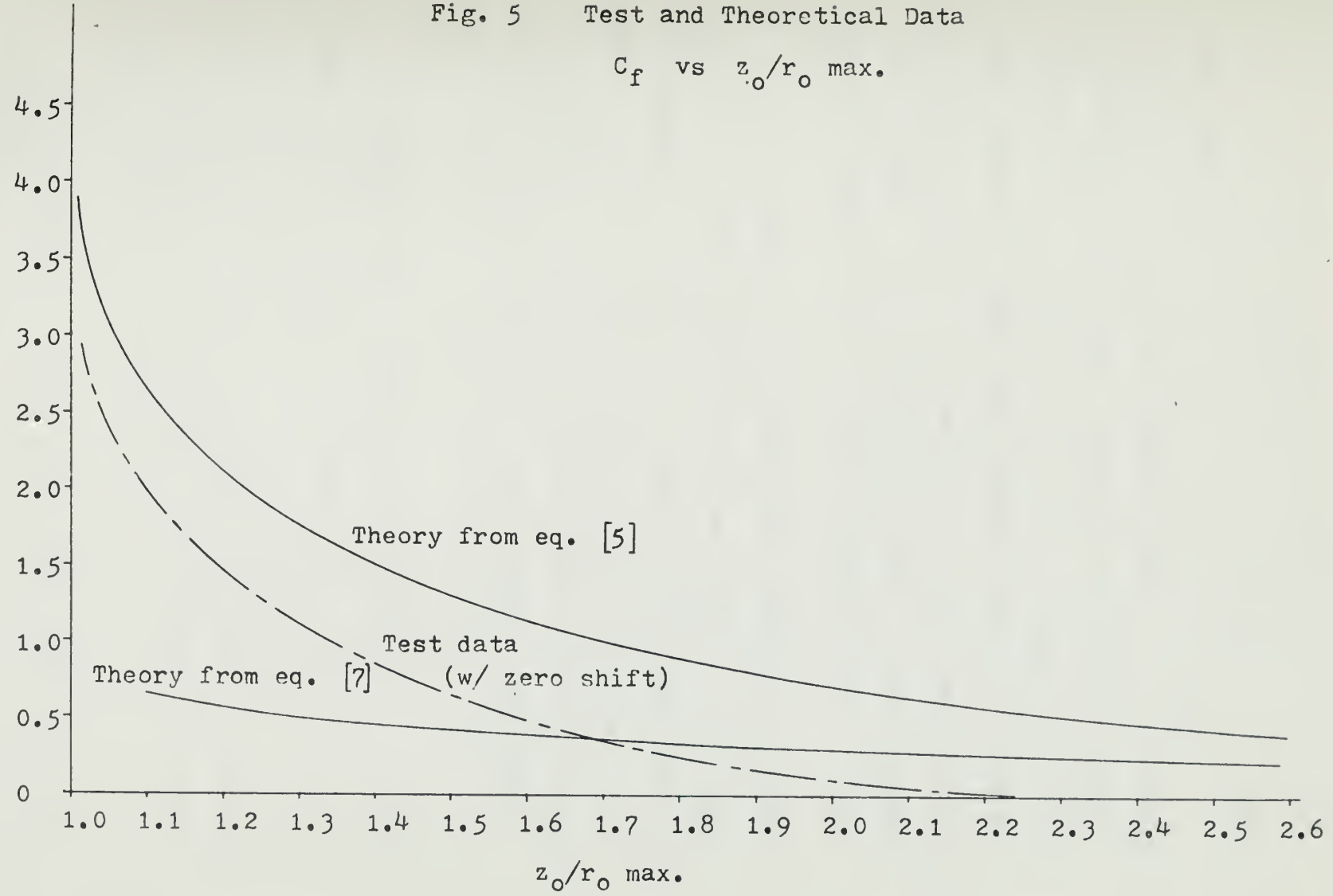

was omitted from evaluation. The supporting arm for the model was located at 40% of the length. All moments were read about this point, as were the forces. In order to isolate the pitching moment, it was necessary to assume that the drag, which also recorded a moment, acted at the centroid of the body. Because the fairing also produced a drag, this was not the case. This assumption estimates the moment at a larger value than actually exists. Subtraction of it from the total moment, however, still leaves a sizable negative pitch torque.

If the sign of the moment had changed as the sign of the lift force changed, the two could be considered in agreement. However, the value of the moment was always negative. This discrepency would make any shift of the moment and force acting at the strut to the mid-chord to conform with theory meaningless. The moment data, therefore, is only included in Appendix 2.

Reference [6] explains the procedure in going from equations [5] and [6] to [7] and [8]. This requires one additional assumption of slender body theory. This last approximation allows the quantity in braces in the first two equations to be considered a two dimensional rather than a series of singularities.

Figs. 3 and 4, however, show that there is a large discrepency between the values of C_f and C_m estimated by

the two methods. Furthermore, the shape of experimental curve of C_f more closely fits that of equation [5]. Therefore, this last assumption appears to over simplify the problem for the body tested here.

Section V contains the final conclusions of this report, as well as suggestions for future research in this area.

V. CONCLUSIONS AND RECOMMENDATIONS

If all errors in the system are considered independent of distance from the wall, and the data points of C_f are shifted up so that all values are positive, the values are in close proximity to the theoretical curves. Because the points thus determined fall, for the major part, in the shape of the curve determined by equation [5] , it would be safe to assume the approximation used to derive [7] underestimates the true values by a discernable amount. Thus, the shape tested for this report cannot be considered to act entirely as a slender body.

Results show that an attraction force toward a wall becomes sizable as the body comes close to it, as predicted. Further tests should be conducted before the theory is applied to actual design, however. It is suggested that furure experiments be conducted without a strut between the wall and the body. Every effort should be taken to make sure any interference force is eliminated, such as that due to an angle of attack. Finally, the recording system should be designed to be accurate for the forces involved. A suggested concept is to mount a small range dynamometer within the body so

that only forces acting on the model are recorded. It is hoped that the difficulties encountered in preparing this report will aid those who investigate this problem further.

Besides the subject of the force due to a wall, there are many areas open for study in the field of potential flow as applied to bodies of revolution. One such topic considers the forces on submerged bodies due to surface waves. Here, too, the forces to be measured are small, but the importance of any findings would be of significant value to aid man in controlling his environment.

APPENDIX 1.

DATA REDUCTION

Tihs appendix outlines the method used to reduce the raw data to values which more closely represent the true forces and moments acting on the body. The data chosen is that for the body at a position z_o/r_o max. = 1.02 qith a flow velocity of a 8.0 ft. per sec.

The original output readings were

(L)	LIFT	=	+ 58	counts
(DI)	INNER DRAG	=	- 32	counts
(DO)	OUTER DRAG	=	+ 41	counts

Converting to forces from the calibration we have

DI	=	- 3.62	lbs.
DO	=	+ 2.66	lbs.

for a streamwise force of - .96 lbs. Summing moments about the tunnel wall, the body was determined to be experiencing a negative pitching moment about the wall of - 24.242 in.-lbs. Calibration also determined that lift has a negligible effect on the drag readings, but

drag and moment produce a sizable error in the lift recording. From the known drag and moment the error in the lift cell was 13 counts. Thus

$$L = 71 \text{ counts}$$
$$= 2.585 \text{ lbs.}$$

However, the differential pressure due to the increase in flow speed in the test section was - 79MM of mercury or .677 lbs. Therefore, the total lift force was 3.260 lbs.

Since the drag produces a moment at the wall, this was calculated as - 1.707 in.-lbs. Thus the net moment due to the lift force was - 22.535 in.-lbs.

However, all force readings did not return to zero at zero flow speed. Assuming a linear zero shift throughout the run, the lift force to be considered was corrected to 3.334 lbs.

APPENDIX 2.

This addendum contains the experimental values of F_z and M_y recorded for report in this paper. It should be noted that the lift forces have been corrected for a zero shift so that they could be used in computing the C_f data. The moment values, however, have not been so altered. It must be remembered that the results represent a moment about the supporting shaft, located at 0.40 L, or 9.80 inches from the nose of the body. Positive moment indicates a counter clockwise torque about the y-axis.

A. Values of F_z versus flow velocity.

U	F	U	F
0	0	0	0
11.4	.184	10.7	.134
12.3	.221	11.9	.147
12.9	.242	13.3	.196
13.9	.219	14.5	.347
14.9	.386	15.8	.525
15.8	.326	17.0	.604
16.9	.349	18.1	.636
17.4	.405	18.6	.684
18.5	.465	17.9	.662
17.7	.379	17.1	.604
17.7	.379	15.6	.388
16.9	.257	14.6	.301
15.6	.169	13.3	.152
14.8	.167	12.0	.166
13.3	.094	10.9	.098
12.4	.034	0	0
11.5	.086		
10.5	.082		
0	0		

TABLE XIX. F_z at z_o/r_o max. = 2.43

TABLE XX. F_z at z_o/r_o max. = 2.32

$\frac{U}{-}$	$\frac{F_z}{-}$
0	0
10.7	.195
12.2	.292
13.4	.351
14.4	.392
15.4	.422
16.9	.467
18.0	.253
18.0	.253
18.6	.018
0	0

TABLE XXI. F_z for z_o/r_o max. = 2.14

$\frac{U}{-}$	$\frac{F_z}{-}$
0	0
10.7	.142
12.0	.209
13.1	.277
14.4	.309
15.9	.489
16.9	.186
18.0	.082
18.6	-.034
17.9	-.044
15.8	-.128
14.4	-.207
13.0	-.121
12.0	-.127
10.7	-.148
0	0

TABLE XXII. F_z for z_o/r_o max. = 2.02

U	F_z	U	F_z
0 ft/sec	0 lbs.	0 ft/sec	0 lbs.
10.7	.052	10.5	-.057
12.1	.118	11.8	-.108
13.1	.140	13.0	-.159
14.6	.210	14.3	-.054
15.6	.279	15.5	+.006
16.7	.557	16.7	.122
18.0	.372	18.0	.218
18.6	.363	18.6	.247
18.0	.427	18.0	.181
16.7	.448	16.7	.148
15.4	.443	15.5	.079
14.6	.555	14.3	.002
13.1	.305	13.0	.007
12.1	.613	11.8	.003
10.7	.225	10.5	.018
0	0	0	0

TABLE XXIII. F_z for z_o/r_o max. = 1.89

TABLE XXIV. F_z for z_o/r_o max. = 1.79

U	F_z	U	F_z
0 ft/sec	0 lbs.	0 ft/sec	lbs.
10.5	+.005	10.5	-.358
11.8	-.046	11.8	-.383
13.0	-.052	13.0	-.460
14.3	+.035	14.3	-.539
15.5	+.132	15.5	-.569
16.7	+.082	16.7	-.655
18.0	+.107	18.0	-.785
18.6	+.075	18.6	-.855
18.0	+.044	18.0	-.840
16.7	+.056	16.7	-.700
15.5	+.047	15.5	-.660
14.3	+.028	14.3	-.601
13.0	+.013	13.0	-.524
11.8	+.093	11.8	-.491
10.5	+.007	10.5	-.431
0	0	0	0

TABLE XXV. F_z for z_o/r_o max. = 1.64

TABLE XXVI. F_z for z_o/r_o max. = 1.51

U	F_z	U	F_z
0 ft/sec	0 lbs	0 ft/sec	0 lbs.
10.5	-.403	10.5	-.140
11.8	-.454	11.8	-.264
13.0	-.577	13.0	-.442
14.3	-.690	14.3	-.719
15.5	-.776	15.5	-.713
16.7	-.769	16.7	-.708
18.0	-.827	18.0	-.875
18.6	-.878	18.6	-.863
18.0	-.809	18.0	-.775
16.7	-.787	16.7	-.599
15.5	-.675	15.5	-.540
14.3	-.542	14.3	-.498
13.0	-.585	13.0	.377
11.8	-.545	11.8	-.299
10.5	-.438	10.5	-.367
0	0	0	0

TABLE XXVII. F_z for z_o/r_o max. = 1.39

TABLE XXVIII. F_z for z_o/r_o max. = 1.29

$\frac{U}{-}$	$\frac{F_z}{-}$	$\frac{U}{-}$	$\frac{F_z}{-}$
0 ft/sec	0 lbs.	0 ft/sec	0 lbs.
10.5	-1.121	10.5	- .614
11.8	-1.355	11.8	- .611
13.0	-1.653	13.0	- .725
14.3	-2.084	14.3	- .893
15.5	-2.416	15.5	-1.105
16.7	-2.875	16.7	-1.264
18.0	-3.334	18.0	-1.448
18.6	-3.631	18.6	-1.546
18.6	-3.514	18.6	-1.600
18.0	-3.353	18.0	-1.494
16.7	-2.794	16.7	-1.282
15.5	-2.435	15.5	-1.105
14.3	-2.031	14.3	- .864
13.0	-1.690	13.0	- .651
11.8	-1.448	11.8	- /526
10.5	-1.151	10.5	- .423
0	0	0	0

TABLE XXIX. F_z for z_o/r_o max. = 1.18

TABLE XXX. F_z for z_o/r_o max. = 1.02

B. Values of M_y versus flow velocity.

U	M_y	U	M_y
0 ft/sec	0 in-lbs	0 ft/sec	0 in-lbs
11.4	-11.91	10.7	-11.94
12.3	-13.82	11.9	-11.67
12.9	-14.78	13.3	-15.82
13.9	-17.62	14.5	-17.92
14.9	-20.00	15.8	-21.20
15.8	-23.82	17.1	-23.90
16.9	-26.68	18.1	-26.76
17.4	-28.10	18.6	-27.79
18.5	-31.44	17.9	-22.71
17.7	-28.10	17.1	-20.31
16.9	-25.24	15.6	-17.33
15.6	-21.92	14.6	-16.22
14.8	-18.59	13.3	-13.14
13.3	-15.24	12.0	-10.54
12.4	-13.10	10.9	- 8.36
11.5	-11.90	0	+ .07
10.5	-10.48		
0	- .10		

TABLE XXXI. M_y for z_o/r_o max. = 2.43

TABLE XXXII. M_y for z_o/r_o max. = 2.32

U	M_y
0 ft/sec	0 in-lbs
10.7	- 9.35
12.2	- 9.06
13.4	-13.56
14.4	-14.64
15.4	-17.89
16.9	-22.97
18.0	-25.52
18.6	-27.98
0	+ 1.27

TABLE XXXIII. M_y for z_o/r_o max. = 2.14

U	M_y
0 ft/sec	0 in-lbs
10.7	- 5.26
12.0	- 6.70
13.1	- 8.02
14.4	- 9.65
15.9	-13.92
16.9	-17.46
18.0	-19.89
18.6	-27.41
17.9	-18.95
16.9	-17.51
15.8	-13.71
14.4	-11.28
13.0	- 9.32
12.0	- 8.85
10.7	- 6.38
0	+ 1.31

TABLE XXXIV. M_y for z_o/r_o max. = 2.02

$\frac{U}{U_0}$	$\frac{M_y}{M_{y_0}}$	$\frac{U}{U_0}$	$\frac{M_y}{M_{y_0}}$
0 ft/sec	0 in-lbs	0 ft/sec	0 in-lbs
10.7	-12.96	10.5	- 9.16
12.1	-11.44	11.8	- 9.81
13.1	-12.82	13.0	-11.20
14.6	-14.37	14.3	-12.06
15.6	-17.03	15.5	-15.03
16.7	-15.21	16.7	-16.77
18.0	-18.55	18.0	-18.84
18.6	-19.87	18.6	-19.54
18.0	-16.90	18.0	-16.95
16.7	-14.22	16.7	-15.63
15.4	-12.42	15.5	-12.44
13.1	-10.30	13.0	- 8.99
12.1	- 7.67	11.8	- 7.12
10.7	- 8.28	10.5	- 5.51
0	- 3.10	0	- 1.56

TABLE XXXV. M_y for z_o/r_o max. = 1.89

TABLE XXXVI. M_y for z_o/r_o max. = 1.79

U —	M_y —	U —	M_y —
0 ft/sec	0 in-lbs	0 ft/sec	0 in-lbs
10.5	- 4.72	10.5	- 8.46
11.7	- 9.51	11.7	- 8.84
13.0	- 9.49	13.0	- 9.96
14.3	-13.09	14.3	-13.63
15.5	-17.35	15.5	-17.67
16.7	-18.89	16.7	-17.71
18.0	-18.07	18.0	-19.29
18.6	-22.16	18.6	-21.03
18.0	-19.58	18.0	-19.18
16.7	-16.67	16.7	-15.87
15.5	-14.72	15.5	-14.76
14.3	-11.62	14.3	-12.17
13.0	-11.30	13.0	-10.68
11.7	- 7.80	11.7	- 9.21
10.5	- 7.87	10.5	- 7.00
0	- 7.56	0	-13.06

TABLE XXXVII. M_y for z_o/r_o max. = 1.64

TABLE XXXVIII. M_y for z_o/r_o max. = 1.51

$\frac{U}{-}$	$\frac{M_y}{-}$	$\frac{U}{-}$	$\frac{M_y}{-}$
0 ft/sec	o in-lbs	0 ft/sec	0 in-lbs
10.5	- 7.81	10.5	- 6.72
11.8	- 8.76	11.8	- 7.88
13.0	-11.38	13.0	- 9.34
14.3	-11.66	14.3	-13.13
15.5	-15.02	15.5	-12.91
16.7	-18.06	16.7	-16.72
18.0	-20.32	18.0	-18.95
18.6	-20.32	18.0	-18.95
18.6	-20.70	18.6	-19.34
18.0	-18.87	18.0	-17.49
16.7	-17.30	16.7	-15.17
15.5	-14.63	15.5	-10.49
14.3	-11.67	14.3	-12.05
13.0	-11.72	13.0	-10.89
11.8	-10.41	11.8	- 8.66
10.5	- 8.03	10.5	- 5.56
0	- 2.23	0	- 3.91

TABLE XXXIX. M_y for z_o/r_o max. = 1.39

TABLE XL. M_y for z_o/r_o max. = 1.29

U	M_y	U	M_y
0 ft/sec	0 in-lbs	0 ft/sec	0 in-lbs
10.5	- 5.04	10.5	-10.00
11.8	- 7.55	11.8	-11.71
13.0	- 8.09	13.0	-13.35
14.3	-11.07	14.3	-15.11
15.5	-13.00	15.5	-17.80
16.7	-13.44	16.7	-19.44
18.0	-15.90	18.0	-22.54
18.6	-15.96	18.6	-23.57
18.6	-15.96	18.6	-22.72
18.0	-15.04	18.0	-21.49
16.7	-12.08	16.7	-17.76
15.5	-10.32	15.5	-14.97
14.3	- 8.93	14.3	-12.39
13.0	- 6.34	13.0	-10.11
11.8	- 5.14	11.8	- 7.86
10.5	- 4.32	10.5	- 7.13
0	+ .30	0	- .93

TABLE XLI. M_y for z_o/r_o max. = 1.18

TABLE XLII. M_y for z_o/r_o max. = 1.02

WORKS CITED

1 M. Lagally, "Berechnung der Krafte und Momente, die strömende Flüssigkeiten auf ihre Begrenzung ausüben." Zeitschrift für Angewandte Mathematik und Mechanik, Band 2, Heft 6, December 1922.

2 W. E. Cummins, "The Force and Moments Acting on a Body Moving in an Arbitrary Potential Stream," DTMB Report 708, 1953 (also Journal of Ship Research, vol. 1, April 1957).

3 L. Landweber and Matilde Macagno, "Force on a Prolate Spheroid in an Axisymetric Potential Flow", Journal of Ship Research, vol 8, no. 1, June 1964.

4 Phillip Eisenberg, "An approximate Solution for Incompressible Flow About an Ellipsoid Near a Plane Wall," Journal of Applied Mechanics, vol. 17, pp 154-158, 1950.

5 E. A. James, "Flow Over a Shadow Body Translating Near a Wall," delivered to the Los Angeles Metropolitan Section of the Society of Naval Architects and Marine Engineers, 1969.

6 J. Nicholas Newman, "The Force and Moment on a Slender Body of Revolution Moving Near a Wall," DTMB Report 2127, December 1965.

FOOTNOTE

1 Bryan Thwaites, Incompressible Aerodynamics, Oxford Press, 1960, pp. 405-409.